ACS APPLIED MATERIALS & INTERFACES

Research Article

www.acsami.org

Improving the Energy Density and Power Density of CF_x by Mechanical Milling: A Primary Lithium Battery Electrode

M. Anji Reddy,*[,†] Ben Breitung,[†] and Maximilian Fichtner[†,‡]

[†]Institute of Nanotechnology (INT), Karlsruhe Institute of Technology (KIT), Hermann-von-Helmholtz-Platz 1, 76344 Eggenstein-Leopoldshafen, Germany

[‡]Helmholtz Institute Ulm (HIU), Albert-Einstein-Allee 11, 89081 Ulm, Germany

ABSTRACT: The effect of high energy ball milling on the electrochemical performance of graphite fluoride (CF_x) was investigated. A significant improvement was observed in both energy density and power density. The volumetric energy density was increased up to a factor of 3 with ball milled materials compared with pristine materials. The gravimetric energy density was increased up to a factor of 2, depending on the discharge rates. At 6C the ball milled material still delivered 40% of its nominal capacity, whereas the pristine material did not exhibit any capacity any more. We achieved the power density of 9860 W/kg with a gravimetric energy density of 800 Wh/kg for the optimized material.

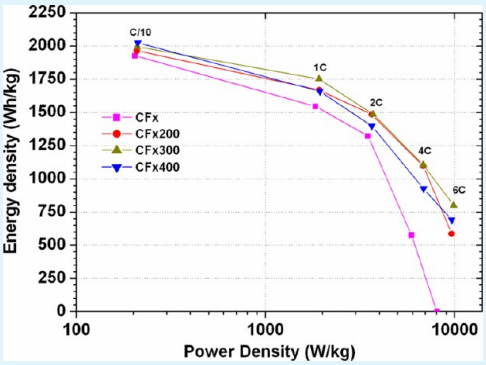

KEYWORDS: *Li/CF_X primary battery, mechanical milling, high power density, high energy density*

INTRODUCTION

Primary batteries are an important class of energy storage devices whose applications span from portable electronics to mining, defense, and implantable medical devices. Among the various primary battery technologies, lithium based batteries offer high energy density. In particular, Li/CF_x primary batteries offer high theoretical capacity compared with other primary batteries, such as Li/$SOCl_2$ and Li/MnO_2, which makes them suitable for long operating and small medical devices, for example.[1] However, the power density of the Li/CF_x battery is low, and the battery cannot be used for high drain applications. Considerable efforts have been made to understand and improve the electrochemical performance of the Li/CF_x system.[2,3] Equation 1 describes the discharge reaction of the Li/CF_x primary battery. The discharge reaction involves the formation of carbon and insulating LiF. The precipitation of LiF impedes the progress of the discharge reaction.

$$CF_x + x\mathrm{Li} \rightarrow \mathrm{C} + x\mathrm{LiF} \quad (1)$$

Thus the Li/CF_x battery delivers its theoretical specific capacity only when the battery is discharged at low rates. At high discharge rates the discharge capacity and discharge voltage decrease dramatically. Thus, the power density of the Li/CF_x primary battery needs to be improved, and various approaches have been tried in that respect. As the frequently used graphite mono fluoride (CF_x, $x \sim 1$) is an electrical insulator, most of the research has been performed to improve the electronic conductivity of CF_x, for example, by addition of conductive carbon, or oxides,[4−9] or by using partially or subfluorinated carbon materials (CF_x, $x < 1$) to provide intrinsic electronic conductivity.[10−12] However, while the subfluorinated carbon materials offer an improved power density, their theoretical specific capacity is low because of the lower amount of F.[10−12]

Herein for the first time we demonstrate that pretreating the CF_x by high energy ball milling leads to a material with reduced particle size and altered physical and electrochemical properties. Interestingly, both volumetric energy density and power density of CF_x are improved considerably compared with the pristine sample while the specific capacity remains unaffected.

EXPERIMENTAL SECTION

The CF_x sample was purchased from Sigma Aldrich. The carbon content in the sample was estimated by elemental analysis, and the composition was determined as $CF_{1.1}$. Ball milling of $CF_{1.1}$ was done using tungsten carbide vial and balls. The sample was milled at 200, 300, and 400 rpm for 2 h, with a ball to powder ratio of 24:1. The samples are labeled as CF_x, CF_x 200, CF_x 300, and CF_x 400 for pristine, ball milled at 200, 300, and 400 rpm, respectively. Powder X-ray diffraction (PXRD) patterns were recorded in the 2θ range 5−70° using a Bruker D8 Advance diffractometer equipped with Cu K_α radiation. Scanning electron microscopy (SEM) was performed with a LEO 1530 at 15 keV using carbon tape as substrate. Nitrogen−physisorption measurements were conducted with a Micromeritics ASAP 2020 system at 77 K. Prior to measurements the samples were degassed at 150 °C for 12 h in vacuum. Pore size distributions were calculated based on a DFT model assuming slit-shaped pores. The specific surface area was determined according to the Brunauer−Emmett−Teller (BET) theory.

Electrochemical studies were performed in Swagelok type cells. Electrode fabrication and assembly of electrochemical cells was done in

Received: August 16, 2013
Accepted: October 3, 2013
Published: October 3, 2013

an argon filled glovebox. The electrodes were fabricated by mixing active material, acetylene black, and poly vinylidene fluoride-hexafluoro propylene (PVDF-HFP) in the mass ratio of 70:20:10. A slurry containing the above mixture was prepared by using *N*-methyl-2-pyrrolidinone, spread on a stainless steel (SS) foil (area: 1.13 cm^2), and dried on a hot plate at 160 °C for 12 h. Typically, each electrode contained 2−3 mg of the active material. Lithium foil (Goodfellow, 99.9%) was used as the negative electrode, and a borosilicate glass fiber sheet saturated with 1 M $LiPF_6$ in 1:1 ethylene carbonate (EC)/dimethyl carbonate (DMC) (LP30, Merck) was used as separator and electrolyte. The cells were placed in an incubator (Binder) to maintain a constant operation temperature of 25 °C. The electrochemical studies were carried out using Arbin battery cycling unit. The tap density of the powders was measured using a volumetric tube. A quantity of material is passed through the tube and gently taped. The material filled until a marked volume is weighed to determine the tap density of the powder. The measurement was repeated three times, and the average value is given.

RESULTS AND DISCUSSION

Figure 1 shows the powder XRD patterns of pristine CF_x and ball milled CF_x 200, CF_x 300, and CF_x 400 samples. The pristine CF_x is phase pure, and no graphite peaks are seen in the XRD. After ball milling a slight broadening of the peaks is observed. Figure 2 shows the SEM images of the CF_x, CF_x 200, CF_x 300, CF_x 400 samples. The pristine CF_x exhibited flake like morphology with layered type structure. Particle sizes are in the range of 1−10 μm. Ball milled CF_x samples showed more irregular morphology and no visible layered structure. In ball milled samples milling resulted in smaller crystallite size but led to larger agglomerate size. In the case of ball milled CF_x samples the agglomerate size was in the range of 0.2−20 μm. However, the crystallite size of the ball milled materials could not be quantified due to the strong agglomeration. To assess the microstructural changes we performed BET analyses of all samples. Figure 3 shows the cumulative pore volume and differential pore volume as a function of pore width measured at 77 K. The BET surface area increased from 213 $m^2\ g^{-1}$ to 267 $m^2\ g^{-1}$ during ball milling. The differential pore volume shows that ball milled samples contained fewer micropores but more mesopores which led to an increase of the total pore volume from 0.1 to up to 0.148 $cm^3\ g^{-1}$. The tap density of ball milled CF_x samples increased more than three times compared with that of the pristine CF_x sample. Obviously, a densification takes place during ball milling which overrates the increasing micro-/mesopore volume considerably. In the case of sample ball milled at 300 rpm, a tap density of 1.07 g cm^{-3} was obtained which is half that of the theoretical density of CF_x (2.82−2.88 g cm^{-3}, for CF_1).[13] Various physical parameters of pristine and ball milled CF_x samples are given in Table 1.

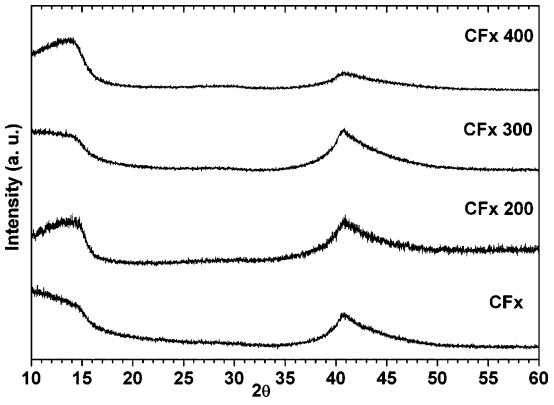

Figure 1. XRD patterns of CF_x samples.

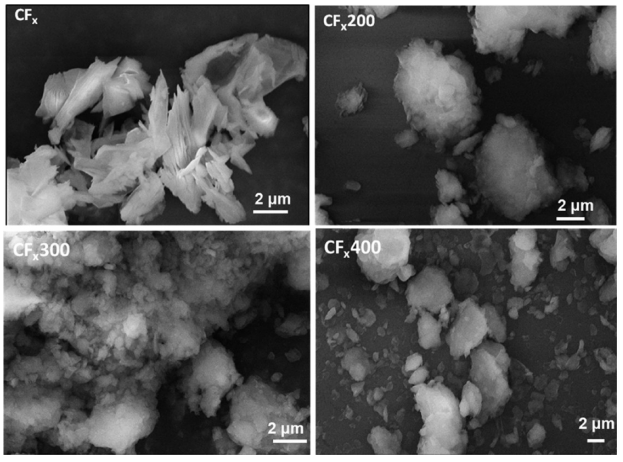

Figure 2. SEM images of CF_x samples before and after ball milling.

Table 1. Physical Parameters of the CF_x Samples before and after Ball Milling

sample	BET surface area ($m^2\ g^{-1}$)	cumulative pore volume ($cm^3\ g^{-1}$)	tap density (g cm^{-3})
CF_x	213.15	0.096	0.30
CF_x 200	285.21	0.148	0.92
CF_x 300	265.76	0.135	1.07
CF_x 400	267.38	0.139	1.02

Figure 4 shows the electrochemical discharge curves of pristine and ball milled CF_x samples obtained at different current densities. The theoretical specific capacity of $CF_{1.1}$ is 896 mA h g^{-1} by assuming the electrochemical reaction of 1.1 Li. The discharge capacities were calculated based on the active material mass in the electrodes. In the case of pristine sample (CF_x), the discharge curve obtained at C/10 shows two plateaus centered at 2.43 and 2.30 V (the average voltage plateaus are obtained by differential capacity plot). Generally, CF_x reacts at a single voltage plateau.[2] The two plateaus observed here are attributed to the inhomogeneous particle size or the reaction of kinetically hindered regions due to the bigger particle size of pristine CF_x.

However, ball milling broke bigger particles into smaller particles, and evidently all ball milled samples exhibited a single voltage plateau. The discharge capacity of all the samples discharged at the C/10 rate was almost equal; nevertheless, the average discharge voltage increased considerably from pristine CF_x (2.27 V) to CF_x 400 (2.35 V), which suggests improved kinetics in the case of the ball milled samples. The theoretical capacity was not achieved which we attribute to the presence of inactive, residual ($-CF_2$). Recently, Greenbaum et al. studied the chemical and electrochemical reaction mechanism of lithium with CF_x by using ^{19}F and the ^{13}C MAS NMR.[3,4] They concluded that at least one type of $-CF_2$ species remained as such during the entire lithiation process of CF_x, indicating either electrochemically isolated regions or an electrochemically inactive bonding type.[3,4] These studies support our assumption of inactive $-CF_2$, which contributes to the total fluorine content but not to the capacity. When discharged at a 1C rate, the voltage dropped to 2.04 V, at a discharge capacity of 753 mA h g^{-1}.

In comparison to pristine CF_x all the ball milled samples exhibited a higher discharge voltage of 0.1 V, with a marginal

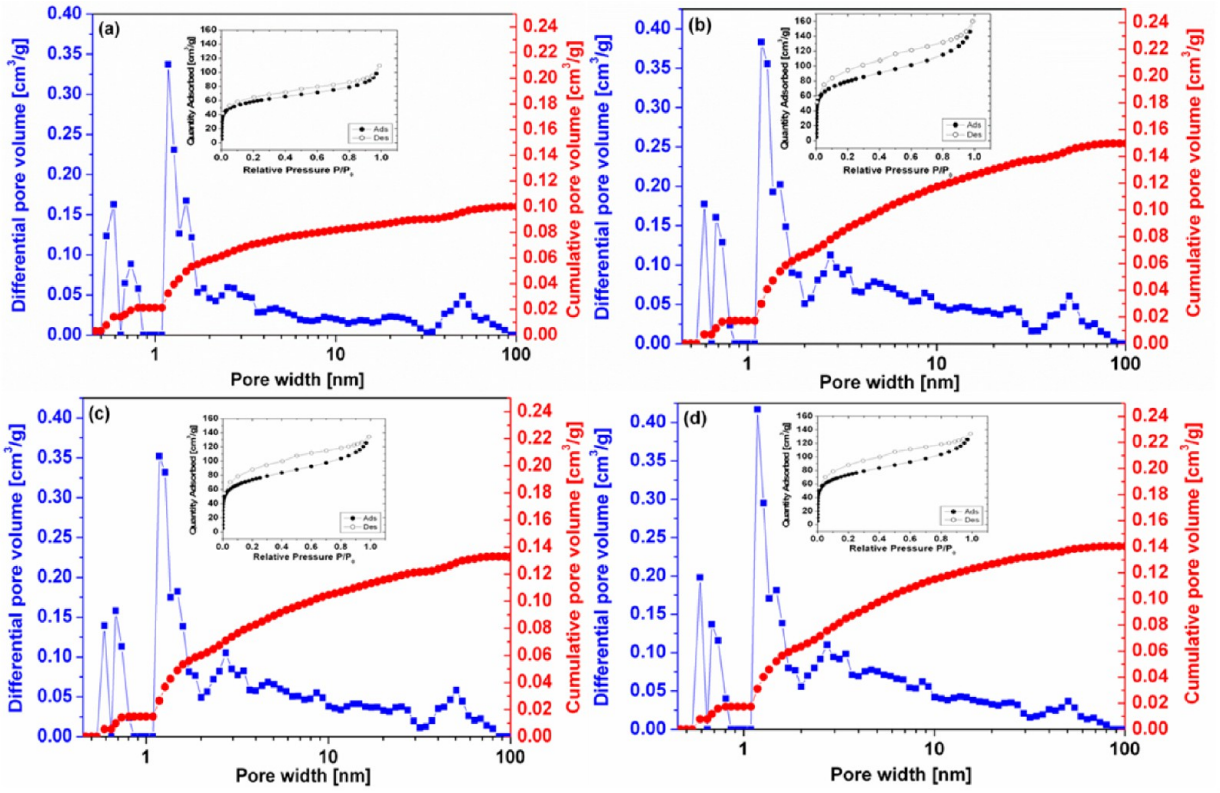

Figure 3. Cumulative pore volume and differential pore volume as a function of pore width measured at 77 K (a) CF_x pristine, (b) CF_x 200, (c) CF_x 300, and (d) CF_x 400. The insets show the respective N_2 isotherm.

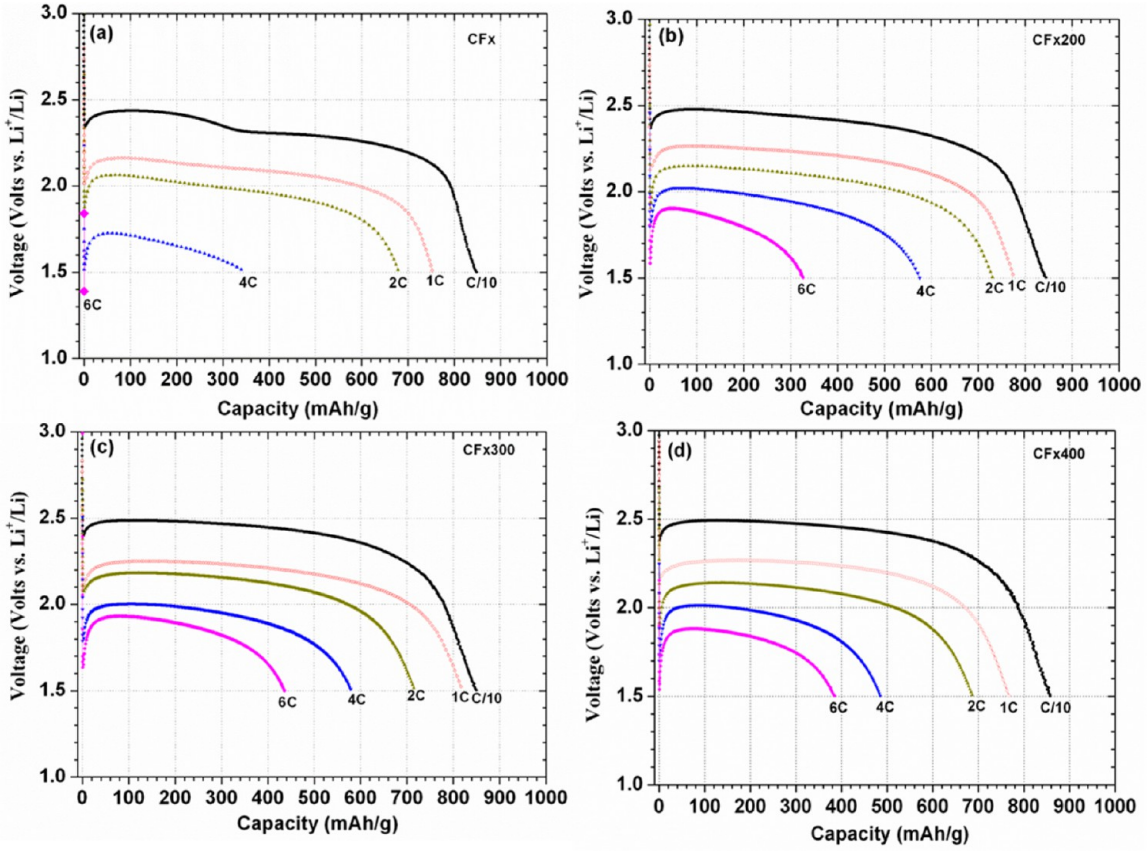

Figure 4. Discharge curves of (a) pristine CF_x, (b) CF_x 200, (c) CF_x 300, and (d) CF_x 400 obtained at different current densities.

dx.doi.org/10.1021/am403438m | ACS Appl. Mater. Interfaces 2013, 5, 11207−11211

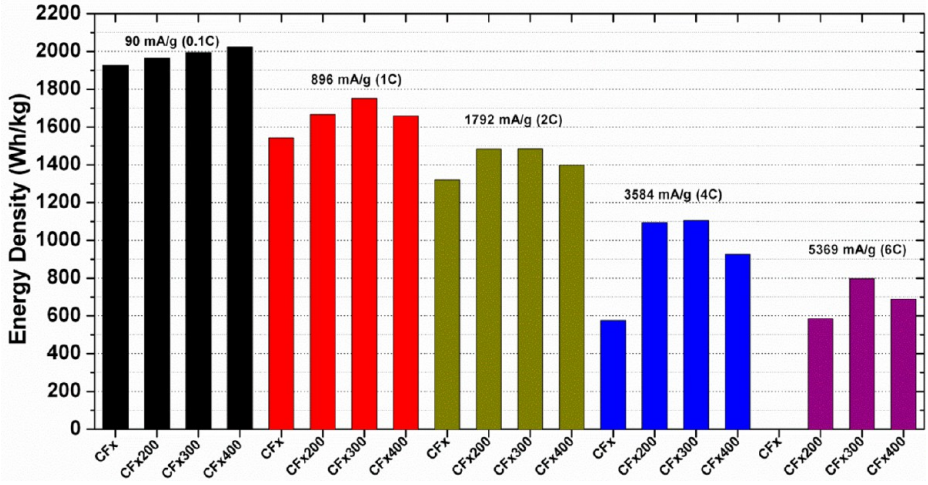

Figure 5. Gravimetric energy densities of CF_x samples at different current densities.

increase in specific capacity. Even at a 2C rate only a marginal change was observed in the discharge capacity and voltage. However, at a 4C rate there was a drastic decrease in the voltage and specific capacity in the pristine sample compared to the ball milled samples which is reflected in the energy density values. The gravimetric energy densities at various C rates are compared for all the samples in Figure 5. The energy density was almost doubled for ball milled sample at a 4C rate compared with that of the pristine sample. At a 6C rate, the pristine sample has no countable capacity in the studied voltage window whereas the ball milled samples exhibited energy densities above that of the pristine sample's energy density at a 4C rate. Figure 6 shows energy density versus power density (Ragone plot) of all CF_x samples studied. Among the balled milled samples CF_x 300 exhibited the best performance.

If the decrease in the particle size of the CF_x is the reason for the better electrochemical performance an improvement in the electrochemical performance can be expected with increasing the ball milling speed. However, the CF_x 400 sample at a 6C rate still shows less capacity compared with that of CF_x 300. We attribute this effect to the damage of the CF_x crystal structure during ball milling at 400 rpm. During the discharge process, CF_x reacts with Li and form C + xLiF. The electronic conductivity of the as formed carbon depends on the structure of the CF_x used. Ball milling at 400 rpm destroys the graphitic backbone of the CF_x, which in turn influences the electronic conductivity of the carbon formed during the discharge, and hence low rate capability compared with the sample ball milled at 300 rpm. However, the CF_x 400 shows high energy density compared with CF_x 200. Thus, optimum ball milling conditions are necessary to achieve a balance between particle size and power density.

A slow step in the discharge reaction of CF_x could be the diffusion of lithium ions within the layers of CF_x and blocking of the layers by the discharge product LiF would impede the diffusion. Ball milling reduces the particle size of the pristine CF_x and reduces the diffusion path lengths for lithium. Together with the high surface area this may have a beneficial effect in better accommodating the discharge product LiF (as the cumulative pore volume increases).

An unexpected feature of the ball milled CF_x samples is their high tap density. It is known from many application examples that grain refinement by grinding and/or ball milling actually leads to an inflation of the powder volume. By applying mechanical

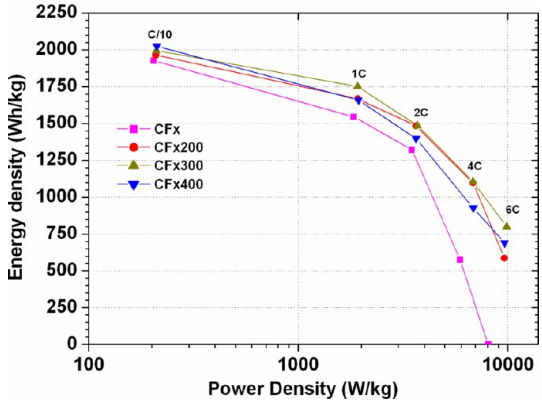

Figure 6. Gravimetric energy density vs power density (Ragone plot).

milling to the CF_x, the particle size was considerably reduced which resulted in a larger BET surface area and an increased total pore volume. During ball milling bigger particles break into smaller crystallites. However, these smaller crystallites again aggregate and rearrange into a different micro structure with small pores and high tap density. Accordingly, the increase in tap density leads to considerable increase in volumetric energy density of the electrodes. Moreover, the increase of both the energy density and the power density is achieved by mechanical milling without losing the high intrinsic specific capacity of the graphite fluoride powder material.

CONCLUSIONS

In conclusion, we showed a simple ball milling approach for the modification of CF_x to achieve high energy density and power density without sacrificing its theoretical specific capacity. We also showed that by ball milling, the tap density could be increased three times to that of pristine CF_x. It is also established that optimized ball milling conditions are necessary to attain high power density.

AUTHOR INFORMATION

Corresponding Author

*E-mail: munnangi.reddy@kit.edu. Phone: 004972160828925.

Notes

The authors declare no competing financial interest.

■ ACKNOWLEDGMENTS

Financial support by State of Baden-Wurttemberg, Project House 'e-drive' (# PHed.L.0208.01) is gratefully acknowledged.

■ REFERENCES

(1) Zu, C. X.; Li, H. *Energy Environ. Sci.* **2011**, *4*, 2614−2624.
(2) Read, J.; Collins, E.; Piekarski, B.; Zhang, S. *J. Electrochem. Soc.* **2011**, *158* (5), A504−A510.
(3) DeSilva, J. H. S. R.; Vazquez, R.; Stallworth, P. E.; Reddy, T. B.; Lehnes, J. M.; Guo, R.; Gan, H.; Muffoletto, B. C.; Greenbaum, S. G. *J. Power Sources* **2011**, *196*, 5659−5666.
(4) Leifer, N. D.; Johnson, V. S.; Ben-Ari, R.; Gan, H.; Lehnes, J. M.; Guo, R.; Lu, W.; Muffoletto, B. C.; Reddy, T.; Stallworth, P. E.; Greenbaum, S. G. *J. Electrochem. Soc.* **2010**, *157* (2), A148−A154.
(5) Li, Y.; Chena, Y.; Fenga, W.; Dingc, F.; Liu, X. *J. Power Sources* **2011**, *196*, 2246−2250.
(6) Zhang, S. S.; Foster, D.; Read, J. *J. Power Sources* **2009**, *188*, 601−605.
(7) Zhang, S. S.; Foster, D.; Read, J. *J. Power Sources* **2009**, *191*, 648−652.
(8) Zhang, Q.; D'Astorg, S.; Xiao, P.; Zhang, X.; Lu, L. *J. Power Sources* **2010**, *195*, 2914−2917.
(9) Meduri, P.; Chen, H.; Chen, X.; Xiao, J.; Gross, M. E.; Carlson, T. J.; Zhang, J. G.; Deng, Z. D. *Electrochem. Commun.* **2011**, *13*, 1344−1348.
(10) Lam, P.; Yazami, R. *J. Power Sources* **2006**, *153*, 354−359.
(11) Yazami, R.; Hamwi, A.; Guerin, K.; Ozawa, Y.; Dubois, M.; Giraudet, J.; Masin, F. *Electrochem. Commun.* **2007**, *9*, 1850−1855.
(12) Read, J. A.; Behl, W. K. *Electrochem. Solid-State Lett.* **2009**, *12*, A16−A18.
(13) Han, S. S.; Yu, T. H.; Merinov, B. V.; van Duin, A. C. T.; Yazami, R.; Goddard, W. A. *Chem. Mater.* **2010**, *22*, 2142−2154.